ORIGINAL RESEARCH

Introducing the Concept of Error Vectors to Improve Source Localization Results of Epileptic Discharges

OPEN

Kanjana Unnwongse,* Carsten H. Wolters,†‡ Tim Wehner,* Lia Theophilo Krüger,* Stefan Rampp,§‖ and Jörg Wellmer*

*Ruhr-Epileptology, Department of Neurology, University Hospital Knappschaftskrankenhaus, Ruhr-University Bochum, Bochum, Germany; †Institute for Biomagnetism und Biosignalanalysis, University of Münster, Münster, Germany; ‡Otto Creutzfeldt Center for Cognitive and Behavioral Neuroscience, University of Münster, Münster, Germany; §Department of Neurosurgery and Department of Neuroradiology, University Hospital Erlangen, Erlangen, Germany; and ‖Department of Neurosurgery, University Hospital Halle (Saale), Halle, Germany.

Purpose: To improve EEG source localization results of interictal epileptic discharges (IED) by applying postprocessing step to electrical source imaging (ESI).

Methods: Localization error of ESI was evaluated in comparison to known sources of stimulation potentials (ESP) by recording simultaneous stereo-EEG/scalp EEG. Error vectors were defined as the offset of the ESI-dipole of ESP to the stereo-EEG contacts used for stimulation. The inverted error vector was applied to the ESI-dipole of IED (IED-dipole).

Results: Seven IED clusters were evaluated. Corrected IED-dipoles were located closer to IED-onset contacts on stereo-EEG than uncorrected IED-dipoles (*median* [*IQR*]: 7.8 [2.5] versus 18.7 [10.7] mm, $P = 0.02$). Anatomically, for high skull conductivities, all corrected IED-dipoles were located in cortical structures or adjacent to epileptogenic lesion, whereas uncorrected IED-dipoles were located in white matter or CSF ($P = 0.02$). Physiologically, cortical extent of IED generators estimated from corrected IED-dipoles was 16.5 cm^2 ($IQR = 10.4$ cm^2) and 7.4 cm^2 (range 5.8–9.2 cm^2) in the group of anterior temporal IED and prefrontal IED, respectively; the former was concordant with the extent estimated by subdural electrodes. In addition, the relationship of stereo-EEG IED amplitude (a) drop with increasing distance (d) from corrected IED-dipole could be modeled as a negative power equation $a(d) \propto 1/d^b$ ($R^2 = 0.87$, $P < 0.01$), with b ranging from 0.79 to 2.3, median: 1.57, consistent with a simulation model of the sensitivity of intracerebral electrode.

Conclusions: Application of inverted error vector reduces localization error and shifts IED-dipole to an anatomically and physiologically plausible location.

Key Words: Epileptic discharge, Generator, Electrical source imaging, Localization error, stereo EEG contact, Presurgical evaluation.

(J Clin Neurophysiol 2025;00: 1–11)

Intracerebral EEG recording is a routine tool in presurgical evaluation for patients with pharmacoresistant epilepsy when noninvasive multimodal workup does not deliver sufficiently conclusive information. It aims at further delineating areas of seizure onset and rate the degree of epileptogenicity in various candidate areas (explorative approach) and to prove epileptogenicity of a lesion or in its immediate vicinity (confirmative approach) or to determine the spatial relationship between seizure onset and functional cortex. Among different intracerebral recording techniques, stereo-EEG offers the unique ability to explore cortical sulci, as well as deep or periventricular areas.[1] Target areas for stereo-EEG electrode placement are determined using information obtained from seizure semiology, neuroimaging, and interictal and ictal scalp EEG recordings.[2] The latter may be subjected to electrical source imaging (ESI), which may strengthen a hypothesis on the localization of the epileptogenic zone in patients with concordant findings in noninvasive modalities. In patients with discordant findings or nonlesional cases, ESI narrows the focus hypothesis and helps to define targets of intracerebral electrode placement.[3]

Few studies provide estimation of sources of epileptic discharges recorded on simultaneous stereo-EEG and scalp EEG using ESI.[4,5] Applying equivalent current dipole localization and distributed source models, sources of ictal epileptic discharges were localized approximately 30 to 47 mm from the ictal onset stereo-EEG contacts. However, these studies were limited by a range of factors influencing spatial accuracy of ESI, such as head surface electrode coverage, spike analysis technique, general limitations of the inverse solution method and forward calculation method, and assumed head tissue conductivities.[6–9]

The authors have no funding or conflicts of interest to disclose.

C. H. Wolters and S. Rampp are supported by the Deutsche Forschungsgemeinschaft (DFG), project WO1425/10-1, and Bundesministerium für Gesundheit, project (ZMI1-2521FSB006), under the frame of European Research Area Personalized Medicine project ERAPERMED2020-227 to C. H. Wolters, L. Theophilo. Krüger was supported by a grant of the Peter and Jytte Wolf foundation.

This paper has been presented at the 16th International Epilepsy Colloquium, Frankfurt am Main on September 20, 2024.

Supplemental digital content is available for this article. Direct URL citations appear in the printed text and are provided in the HTML and PDF versions of this article on the journal's Web site (www.clinicalneurophys.com).

S. Rampp and J. Wellmer share senior authorship.

Address correspondence and reprint requests to Kanjana Unnwongse, MD, Ruhr Epileptologie, Neurologische Klinik, Universitätsklinikum Knappschaftskrankenhaus Bochum, In der Schornau 23-25, 44892 Bochum, Germany; e-mail: kanjana.unnwongse@kk-bochum.de.

Copyright © 2025 The Author(s). Published by Wolters Kluwer Health, Inc. on behalf of the American Clinical Neurophysiology Society. This is an open access article distributed under the terms of the Creative Commons Attribution-Non Commercial-No Derivatives License 4.0 (CCBY-NC-ND), where it is permissible to download and share the work provided it is properly cited. The work cannot be changed in any way or used commercially without permission from the journal.

ISSN: 1537-1603/25/0000-0001
DOI 10.1097/WNP.0000000000001170

In this study, we attempt to improve EEG source localization results in the context of epilepsy presurgical evaluation by applying the principle of the artificial spike (ESI of ESP) model to natural spike (IED) as a "postprocessing" step to ESI. First, individual error vectors were determined for stereo-EEG contacts showing IED onsets based on the ESI-dipole of the ESP at these locations. Then, the inverse of these individual error vectors (iEV) was applied to the ESI-dipole results of the IED. Spatial accuracy of this correction approach was then evaluated.

METHODS

Patient Recordings

Data of 11 patients with pharmacoresistant epilepsy undergoing stereo-EEG evaluation from our previous study were evaluated retrospectively.[10] This study (register number: 20-6970) was approved by the Ethics Commission of the Faculty of Medicine, Ruhr-University Bochum, Germany. Patient selection criterion was a minimum number (>500) of IED recorded with correlates in both stereo-EEG and simultaneous 37-electrode scalp EEG monitoring. Scalp EEG with electrode placement according to the 10-20 system and additional paracentral (FC1/2, FC5/6, CP1/2, CP5/6), inferior frontal-temporal (F11/12, FT9/10 or T1/T2, A1/2, TP9/10), and inferior cerebellar (CB1/2) electrodes was recorded with a sampling rate of 2,000 Hz (Xltek Natus, Middleton). Six patients who had scalp EEG correlates of stereo-EEG IED (7 IED clusters) recorded were included into the study.

Five clusters of anterior temporal IED (distributed on scalp EEG contacts F7/8, F11/12, FT9/10, A1/2 T7/8) were evaluated in four patients (no. 1–4), one with bilateral temporal IED (no. 2) (Fig. 1). All four patients had nonlesional temporal lobe epilepsy based on data obtained during noninvasive evaluation. Stereo-EEG electrodes (AD-tech, Racine, WI) with the diameter of 1.1 mm, contact length of 2.4 mm, and interspacing length of 2.1 mm were used. In two patients (no. 1 and 3), six electrodes were implanted unilaterally into the temporal pole, entorhinal cortex, amygdala, anterior and posterior hippocampus, and the parahippocampal gyrus. In one patient (no. 4), five electrodes were implanted in all aforementioned structures except the temporal pole. In the last patient (no. 2), amygdalae and anterior and posterior hippocampi were implanted bilaterally. Two patients (no. 5 and 6) with prefrontal IEDs (distributed on FP1/2, FC1/2, F3/4, FC5/6, Fz and Cz) had frontal lobe epilepsy in the setting of suspected bottom of sulcus focal cortical dysplasia (FCD) (Fig. 1). In these patients, four and six stereo-EEG electrodes were implanted in the vicinity of the suspected MRI abnormality that had been identified by the Morphometric Analysis Program v2018 (MAP18, kindly provided by *H. J. Huppertz, Swiss Epilepsy Center Zurich, Switzerland*).[11] Mean number of contacts per a stereo-EEG electrode was 9 (range 6–11) for the anterior temporal cluster and 8 (range 4–10) for the prefrontal cluster. For the summary of patient's characteristic (see **Table**, **Supplemental Digital Content** 1, http://links.lww.com/JCNP/A336).

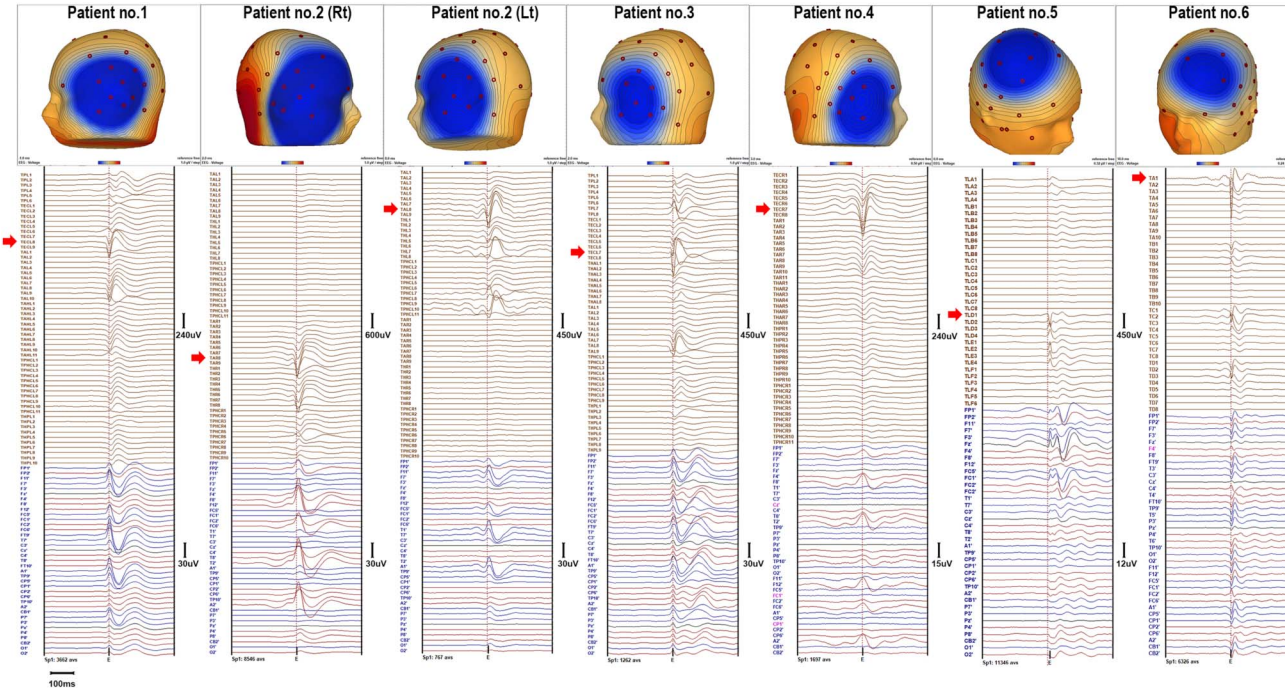

FIG. 1. Seven clusters of averaged scalp EEG correlates of stereo-EEG IED from six patients showing the IED-onset contacts (*red* arrow) recorded on simultaneous stereo-EEG and 37-electrode scalp EEG. Topography (*top* row) display voltage maps at the peak of the IEDs.

IED and ESP Identification

Typical scalp EEG correlates of stereo-EEG IED with comparable onsets and morphology were identified from the first 24 hours of recording by visual inspection using a reference montage. Further IEDs were detected using a template search algorithm (BESA Research 7.1, BESA GmbH, Gräfeling, Germany). Templates, channels, and settings for the automated search were selected manually. Detection results were checked for correctness and excessive additional artifacts. Atypical IED based on visual inspection were rejected. On average, 3,662 (interquartile range: *IQR* 7,194) per IED cluster were detected. Epochs of 250 ms before to 500 ms after the IED peak were then extracted and averaged. The stereo-EEG IED-onset contact was selected by visual inspection as the first contact showing the earliest IED's rising flank (Fig. 2, *right*).

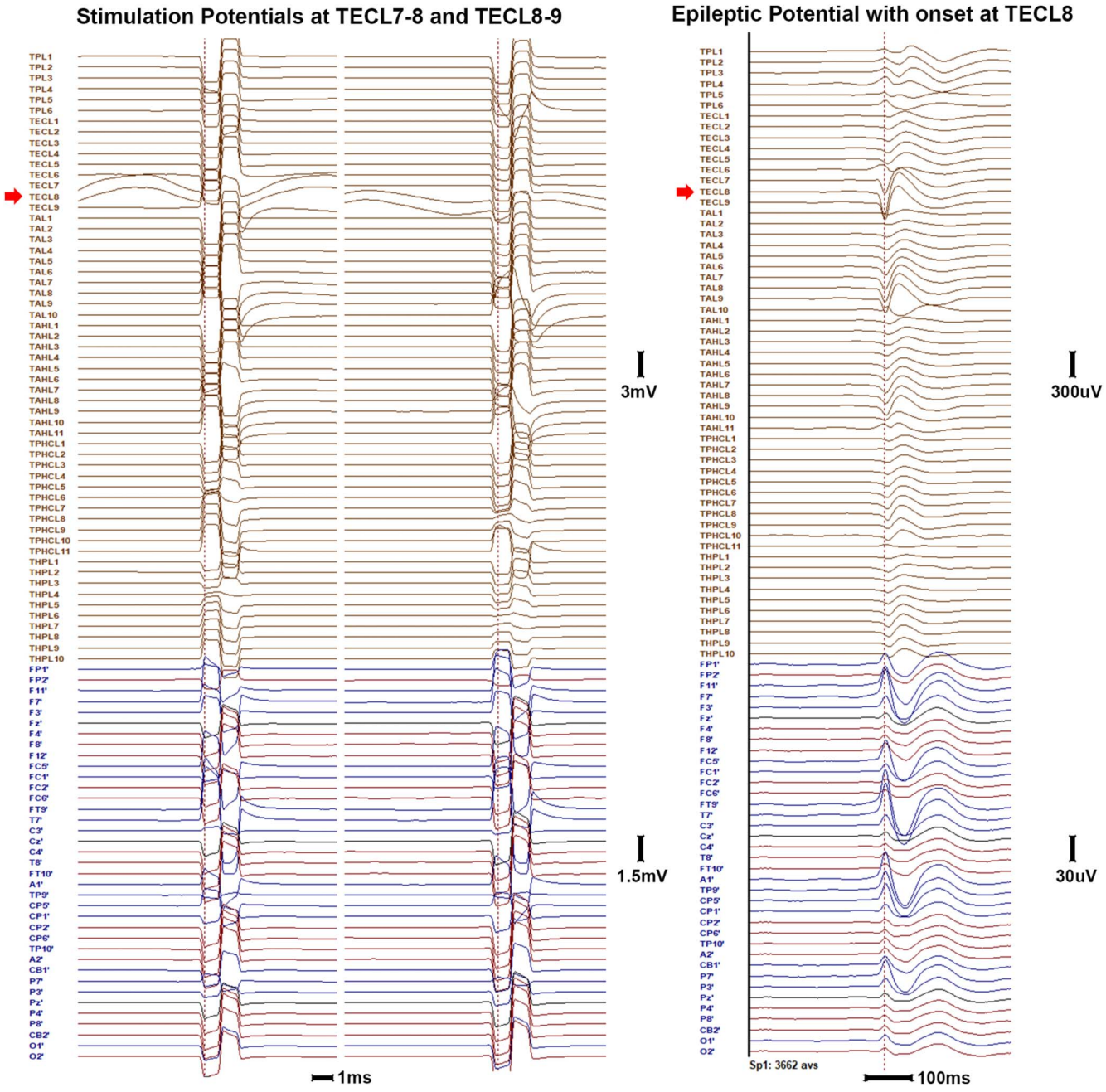

FIG. 2. Left: Averaged scalp EEG correlates of stereo-EEG ESP of stimulated contact pairs (TECL7 and 8, TECL8 and 9) involving the IED-onset contact TECL8 (*red* arrow). Right: Averaged scalp EEG correlates of stereo-EEG IED with onset at contact TECL8 (*red* arrow), recorded on simultaneous stereo-EEG (with reference electrode AF7 and AF8, contacts TPL1 to THPL10 in *brown* lines) and 37-electrode scalp EEG (with reference electrode CPz, contacts FP1-O2 in *blue* and *red* lines).

In our previous study, "bipolar" single pulses (parameters: biphasic square pulse, 2 ms pulse width, 1 mA intensity, 1 Hz) stimulation were applied to pairs of neighboring electrode contacts with a total of 90 to 110 trials per pair (ISIS Stimulator, Inomed Medizintechnik GmbH, Emmendigen, Germany). Scalp EEG correlates of the ESP were recorded with simultaneous stereo-EEG and 37-electrode scalp EEG. For this study, we selected stimulation data involving the IED-onset contacts (Fig. 2*, left*). Epochs of 250 ms before to 500 ms after the ESP were extracted and averaged. The resulting averaged scalp EEG-IED and averaged scalp EEG-ESP were then submitted to ESI.

ESI of ESP and IED as well as Determination and Application of Individual iEV

ESI of averaged scalp EEG-ESP was performed using a single dipole model from the onset to the negative peak (fit interval of −1.5 to 0 ms) of the averaged data. No filters were applied. Regularization of 0 and baseline of −150 to −50 ms was set (BESA Research 7.1, BESA GmbH, Gräfelfing, Germany). In dipole fitting, in each iteration step, the optimizer determines the new positions within the brain compartment, defined during the segmentation of the head volume conductor, with the aim of explaining the data with maximal goodness of fit (BESA MRI 2.0, BESA GmbH, Gräfelfing, Germany). The fit threshold in this study is goodness of fit. Fitted dipoles with goodness of fit of ≥ 80% were included in the analysis. An individual four-compartment finite element method (FEM) model with standard tissue conductivity values of scalp (0.33 S/m), CSF (1.79 S/m), and brain (0.33 S/m) was employed for ESI (BESA MRI 2.0, BESA GmbH, Gräfelfing, Germany). Skull conductivity values were set at the best individual conductivity, providing the smallest localization errors in most contact locations for each patient in our previous study.[10] The optimal skull conductivity was 0.0206 S/m (skull: skin conductivity ratio (SSCR) of 1:16) for patient no. 1, 3, and 6 and 0.0413 S/m (SSCR 1:8) for patients no. 2, 4, and 5. Consequently, ESI-dipoles of the stimulation potentials were obtained.

For the calculation, the averaged scalp EEG-ESP belonging to stimulated contact pairs involving the IED-onset contact was determined. Figure 2 (*left*) shows an example: TECL 8 was the IED-onset contact showing the earliest IED's rising flank. The ESP from contact pairs TECL 7 to 8 and TECL 8 to 9 were both subjected to ESI. The resulting vectors (Fig. 3 *step1*) between the midpoint of the stimulated contact pairs and the ESI-dipole of the stimulation potentials (ESP-dipoles) Eq. 1(1) were then averaged. Correspondingly, this resulted in the individual error vector Eq. 2(2) and averaged ESP-dipole.

Subsequently, ESI of the averaged scalp EEG-IED was performed using the same approach but with a fit interval from the onset to the negative peak of IED. However, because IED data have a considerably lower signal-to-noise ratio than the artificial stimulation potentials, a 0.5 to 40 Hz band pass and a 50 Hz notch filter were applied to mitigate the influence of noise. This resulted in ESI-dipole of IED ("uncorrected IED-dipole") before application of the error vector (Fig. 3*, step2*). The inverse of the individual error vector (iEV) Eq. 3(3) obtained from the earlier step was applied to the uncorrected IED-dipole, resulting in the "corrected IED-dipole" (Fig. 3*, step3*) Eq. 4(4). The mathematic formulation of these calculation is as follows:

$$EV_1 = Coord.\,ESP_{dipole1} - Coord.\,Midpoint\ stimulated\ contact\ pair_1$$
$$EV_2 = Coord.\,ESP_{dipole2} - Coord.\,Midpoint\ stimulated\ contact\ pair_2 \quad (1)$$

$$(EV_1 + EV_2) \div 2 = EV \quad (2)$$

$$(-)EV = iEV \quad (3)$$

$$Coord.Uncorrected\ IED_{dipole} + iEV = Coord.\,Corrected\ IED_{dipole} \quad (4)$$

where Coord. = coordinates.

Application of individual iEV was attempted to correct the localization error, derived from ESI of the IED to improve the source localization results of the IED. We hypothesized that the areas covered by the IED-onset contact on the one hand and the neuronal sources of IEDs on the other hand would be largely overlapping, although not be completely identical in general. Accordingly, we assumed similar tissue environments (regarding conductivity and anisotropy) and depth (in term of distance from the inner skull). Thus, the effect of such influences on localization of ESP-dipole and IED-dipole would be comparable.

All coordinates (IED-onset contact, averaged ESP-dipole, corrected and uncorrected IED-dipoles) were expressed in Talairach space. Euclidean distances from the corrected and uncorrected IED-dipole to the IED-onset and neighboring contacts were evaluated (Fig. 3*, step 3*). The details of electrode localization and Talairach coordinates registration are as follows: Isotropic T1 3D-MPRAGE volume MRI was acquired using a 3T scanner (MAGNETOM Prisma 3.0T, Erlangen, Germany) before implantation of intracranial electrodes. This preimplantation MRI was also used to create an individual FEM model. Postimplantation CT (CT Elekta 1.0, Stockholm, Sweden) was acquired for localizing stereo-EEG and scalp EEG electrodes within 24 hours after implantation. Electrodes were segmented using the postimplantation CT data set. Individual stereo-EEG and scalp EEG contacts were labeled manually according to the clinical documentation. The CT data set was then coregistered to preimplantation MRI using a mutual information approach (Curry 7, Compumedics Neuroscan). The resulting coregistered scalp electrode positions were used for the ESI. The preimplantation MRI was registered in Talairach space, which subsequently allowed expressing electrode localizations from CT in standardized Talairach coordinates.

Plausibility Evaluation of the Corrected IED-Dipole Localization

We expected the corrected IED-dipole to locate closer to the IED-onset contact than the uncorrected IED-dipole. We further evaluated the corrected localization by

1. checking anatomical locations of corrected IED-dipole on individual MRI;
2. estimating the putative cortical extent of the IED generators using the distance from the corrected IED-dipoles to the

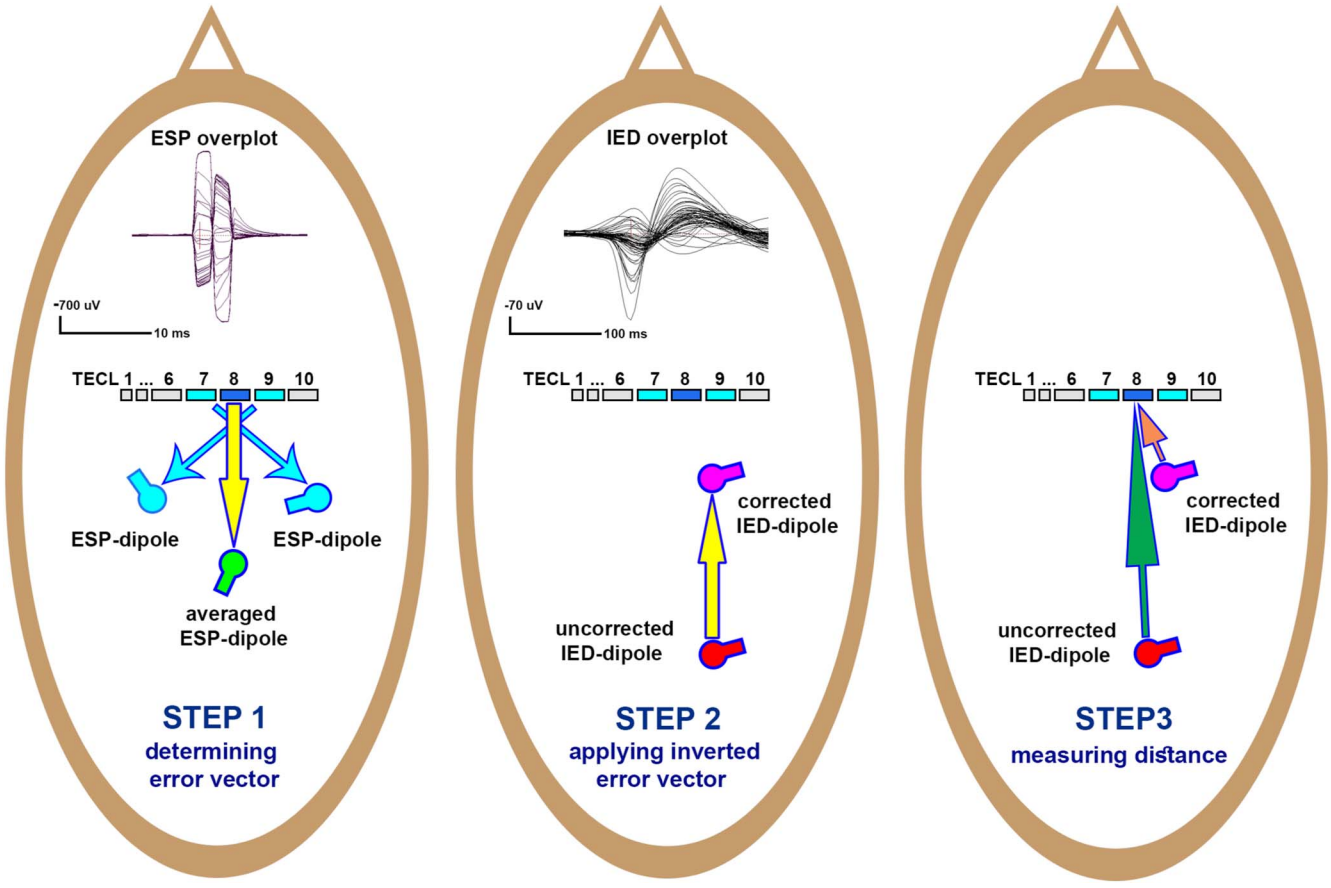

FIG. 3. Workflow of determining and applying the individual iEV. Step 1: The averaged scalp EEG-ESP of stimulated contact pairs (*light blue, ''TECL 7 and 9''*) involving the IED-onset contact (*dark blue, ''TECL 8''*) was subjected to ESI. The resulting vectors (*light blue*) between the midpoint of stimulated contact pairs to ESP-dipoles (*light blue*) were averaged, resulting in the individual error vector (*yellow*) and location of the averaged ESP-dipole (*green*). Step 2: The ESI-dipole of the averaged scalp EEG-IED with stereo-EEG correlates of the earliest IED's rising flank at the IED-onset contact (*dark blue, ''TECL 8''*) was determined (*red*, "uncorrected IED-dipole"). The inverse of individual error vector (iEV) determined in step 1 (*yellow*) was applied (subtracted), resulting in the "corrected IED-dipole" (*magenta*). Step 3: The difference between the location of the IED-onset contact and the "corrected IED-dipole" (*magenta*) and the "uncorrected IED-dipole" (*red*) was determined (*orange/small* and *green/big* arrows respectively).

stereo-EEG contacts recording IED amplitudes above an assumed noise level of approximately 70 μV as a radius to calculate for the cortical involvement;

3. correlating the distance between the corrected/uncorrected IED-dipoles and IED-onset/neighboring contacts to the amplitudes recorded on those contacts by curve fitting. Only contacts with amplitudes ≥ 70 μV were included, assuming that IED below this threshold disappear in background noise. For anterior temporal IED, we used electropositive potentials, recorded by the majority of stereo-EEG contacts sampling from subcortical white matter. The electropositive represents the nonexcited membrane of the soma and basal dendrites in respect to the depolarized apical dendritic membrane, which become extracellularly electronegative during the synaptic excitation of a cortical pyramidal neuron.[12,13] For prefrontal IED, we used electronegative potentials, recorded by most of the contacts sampling from the cortex and the suspected cortical dysplasia. All IED amplitudes were measured using peak analysis (BESA Research 7.1, BESA GmbH, Gräfeling, Germany); and
4. measuring the distance of the corrected IED-dipole to the MRI lesion (patients no. 5 and 6).

Finally, we investigated the effect of varying different skull conductivity values (SSCR) on the determination of the individual iEV and its application to the uncorrected IED-dipole. To this end, the analysis procedure of both averaged scalp EEG-ESP and averaged scalp EEG-IED were repeated, using SSCR from 1:8 to 1:330.

Statistical Analysis

Because of non-normal distribution of the data, median and interquartile range are reported. The correlation between the distance from the corrected IED-dipole to stereo-EEG electrode contacts and IED amplitude was determined using curve estimation with SPSS 16.0 (IBM, New York, NY) to find

a best-fit model. The difference between the distances from corrected and uncorrected IED-dipoles to the IED-onset contact using various skull conductivities were determined using 2-related samples Wilcoxon signed-rank test. The effect of different skull conductivities on the distance from corrected IED-dipole and uncorrected IED-dipole to the IED-onset contact was determined using K-related samples Friedman test. The difference between the anatomical locations of corrected and uncorrected IED-dipoles on individual MRI were determined by Fisher's exact test. Significance was set at $P < 0.05$.

RESULTS

Locations of IED-Dipole before and after Application of the Individual iEV

Five clusters of anterior temporal IED from four patients (one with bilateral temporal IED, no. 2) and two clusters of prefrontal IEDs from two patients (no. 5 and 6) were evaluated. The IED-onset contacts in the patient with prefrontal IED did not only show IED but also ictal epileptic discharge. Median goodness of fit was 94.8% (*IQR* 6.6%) for seven uncorrected IED-dipoles. For 12 locations of ESP-dipole, median goodness of fit was 98.4% (*IQR* 10.1%). In patient no. 2, electrical stimulation data were only available from the stereo-EEG electrodes implanted in the right temporal lobe. We thus mirrored the iEV obtained for the right temporal ESP along the sagittal plane and subsequently applied this mirrored iEV to uncorrected IED-dipole originating in the left temporal lobe. Goodness of fit of uncorrected IED-dipole was 90.5% on the right side and was 90.4% on the left side.

Uncorrected IED-dipoles were located on average 18.7 mm (*IQR* 10.7 mm) from the IED-onset contact. After applying individual iEV, corrected IED-dipoles were located on average 7.6 mm (*IQR* 2.5 mm) from the IED-onset contact. Distances from corrected IED-dipole to the IED-onset contact were significantly shorter than the distances from uncorrected IED-dipoles to the IED-onset contact ($P = 0.02$). In patients no. 5 and 6 with suspected FCD, the distances of IED-dipole to the putative lesion identified by MAP18 on the MRI were 9.8 and 5.6 mm before and 4.5 and 6.6 mm after applying the individual iEV.

Anatomical Locations, Estimated Cortical Extent of IED Generators, and Distance–Amplitude Correlation

While most uncorrected IED-dipoles were located in subcortical white matter areas, we found that all corrected IED-dipoles of the anterior temporal IED cluster were located in cortical or corticosubcortical structures (Fig. 4*, left*). The spacing of stereo-EEG contacts in the temporal lobe provided the opportunity to evaluate stereo-EEG IED amplitudes in relation to the distance from the corrected and uncorrected IED-dipoles (Fig. 4*, right*). We assumed that corrected IED-dipoles better approximate the location of IED sources as their locations were not restricted to the fixed placement and sampling of stereo-EEG electrodes. Assuming noise level of approximately 70 μV, similar to the previous study by Tao et al,[14] we estimated the cortical extent of IED generators, from the corrected IED-dipole. Median cortical extent of IED generators was 16.5 cm^2 (IQR 10.4 cm^2, range 15.1–29.9 cm^2) and 7.4 cm^2 (range 5.8–9.2 cm^2) in the group of anterior temporal IED and prefrontal IED, respectively.

Curve fitting was applied to the distances from corrected and uncorrected IED-dipoles to the IED-onset and neighboring stereo-EEG contacts (d on *x*-axis) in comparison to IED amplitudes (a(d) on *y*-axis) to find the best fit to these correlations. These correlations of corrected IED-dipoles could be fitted well with negative power functions ($a(d) \propto 1/d^b$) (Fig. 5*, left*). The median of R^2, providing a measure of model fit, was 0.87 (*IQR* 0.17). Significance of model fit for corrected IED-dipole to negative power function were $R^2 = 0.87$, $F(1, 14) = 93.2$, $P < 0.01$ in patient no. 1; $R^2 = 0.82$, $F(1, 18) = 83.4$, $P < 0.01$ in patient no. 2(Rt); $R^2 = 0.91$, $F(1,14) = 148.9$, $P < 0.01$ in patient no. 2(Lt); $R^2 = 0.74$, $F(1, 22) = 64$, $P < 0.01$ in patient no. 3; $R^2 = 0.93$, $F(1, 10) = 139.8$, $P < 0.01$ in patient no. 4; $R^2 = 0.75$, $F(1,4) = 12$, $P = 0.03$ in patient no. 5; and $R^2 = 0.88$, $F(1,10) = 74.9$, $P < 0.01$ in patient no. 6. Amplitudes (a) decreased approximately by the inverse of the distances (d) to the power b, with b ranging from 0.79 to 2.3, median 1.57 (*IQR* 0.87). Given higher values of b, IED amplitudes showed a steeper decline with increasing distance. The correlations of uncorrected IED-dipoles varied interindividually and could not be fitted by a common model (Fig. 5*, right*).

Effect of Applying Different Skull Conductivities

We further investigated the effect of varying skull conductivities (SSCR between 1:8 and 1:330) during ESI for averaged scalp EEG-ESP and averaged scalp EEG-IED on the locations of averaged ESP-dipole, individual iEV, and locations of uncorrected and corrected IED-dipoles. Across all examined SSCR, the effect on the distances from corrected IED-dipoles to the IED-onset contacts was insignificant (χ^2 (10, 11) = 15.7, $P = 0.1$, Fig. 6). However, higher skull conductivities i.e., SSCR 1:8 to 1:28 produced significantly larger errors from uncorrected IED-dipoles to the IED-onset contacts (χ^2 (10) = 35.1, $P < 0.001$ for SSCR 1:8; χ^2 (9) = 24, $P = 0.004$ for SSCR 1:16; χ^2 (8) = 19.3, $P = 0.01$ for SSCR 1:24; and χ^2 (7) = 16.1, $P = 0.02$ for SSCR 1:28, Fig. 6). Using SSCR of 1:8 and 1:16, the distances from corrected IED-dipoles to the IED-onset contacts were significantly smaller than from uncorrected IED-dipoles ($Z = -2.2$, $P = 0.03$ for both SSCR, see **Table**, **Supplemental Digital Content 2**, http://links.lww.com/JCNP/A336). Moreover, proportions of corrected IED-dipoles located in cortical or cortico-subcortical structures or adjacent to suspected FCD (patients no. 5 and 6) were significantly higher when using SSCR 1:8 and 1:16 ($P = 0.02$–0.08, see **Figure**, **Supplemental Digital Content 1**, http://links.lww.com/JCNP/A337).

DISCUSSION

By applying individual iEV obtained from electrical stimulation of stereo-EEG contacts, we were able to significantly improve EEG source localization results of IED. In this proof of principle analysis, IED-dipoles shifted closer to an anatomically and physiologically plausible location. For all IED clusters, the

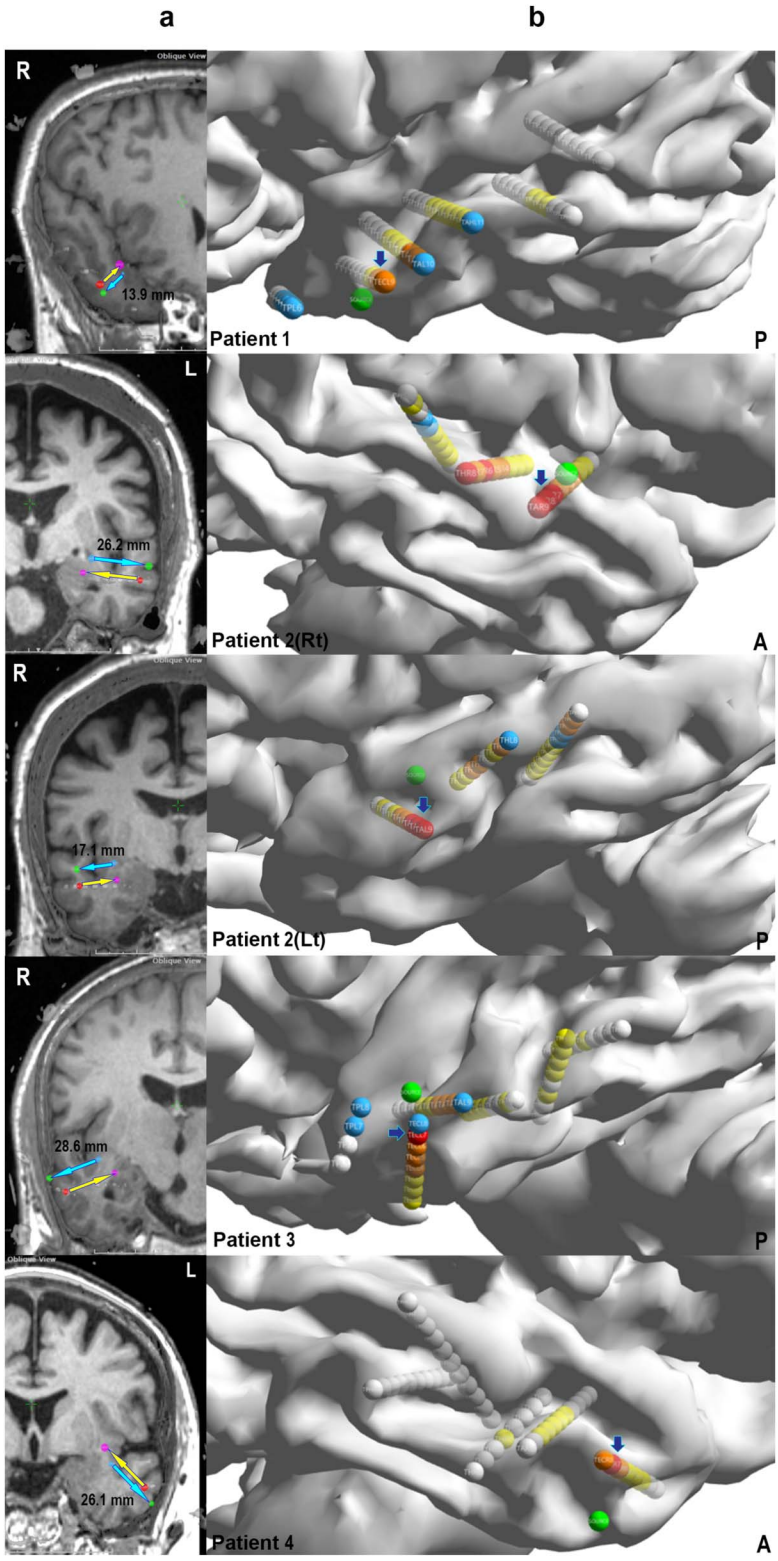

FIG. 4. Spatial relationships between corrected and uncorrected IED-dipoles, averaged ESP dipole and stereo-EEG IED-onset contacts in five temporal clusters derived from patients no. 1–4. Left: Locations of IED-onset contacts in *red*, averaged ESP dipoles in *magenta*, uncorrected IED-dipoles in *blue*, and corrected IED-dipoles in *green* displayed on the individual postoperative CT coregistered to the preoperative T1-weighted MRI. The *yellow/light* arrows represent the individual error vectors, and the *blue/dark* arrows represent the inverse of the individual error vectors (iEV) with their length in millimeters. Right: Locations of corrected IED-dipoles (*green*) and stereo-EEG contacts displayed on surface rendered MRI in different colors, according to the IED amplitudes: *red* for amplitudes >500 μV, *orange* for amplitudes >200–500 μV, *yellow* for amplitudes 70–200 μV, *white* for amplitudes <70 μV, *blue* for electronegative activity. The *dark blue* arrow point at the IED-onset contacts.

localization error between locations of IED-dipole and the IED-onset contact became smaller, the median distance significantly decreased from 18.7 to 7.6 mm. After applying individual iEV, the presumed sites of IED generators were located in cortical or corticosubcortical structures, in contrast to the uncorrected results, which was implausibly located in the subcortical white

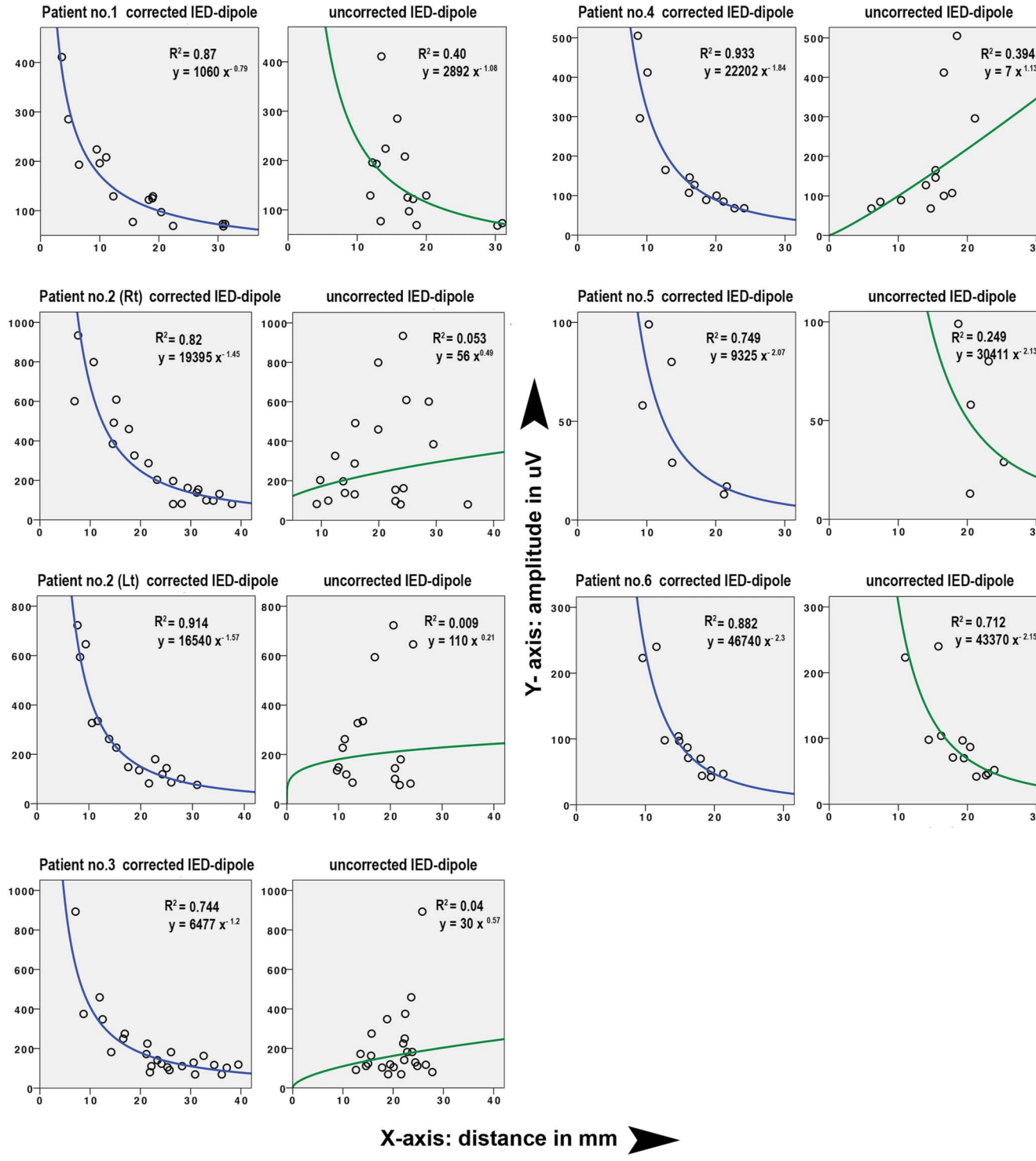

FIG. 5. Correlations of distance from corrected and uncorrected IED-dipoles to the IED-onset contacts (*x-axis*) and IED amplitudes recorded on IED-onset and neighboring contacts (*y-axis*). For the corrected IED-dipoles (*left*), a negative power function could be fitted for all IED clusters. For the uncorrected IED-dipoles (*right*), this was not the case.

matter. Using higher skull conductivities (SSCR 1:8 or 1:16) resulted in closer distances from the corrected IED-dipoles to the IED-onset contacts than SSCR of 1:80, which is applied as a standard tissue conductivity ratio for ESI in the clinical setting.

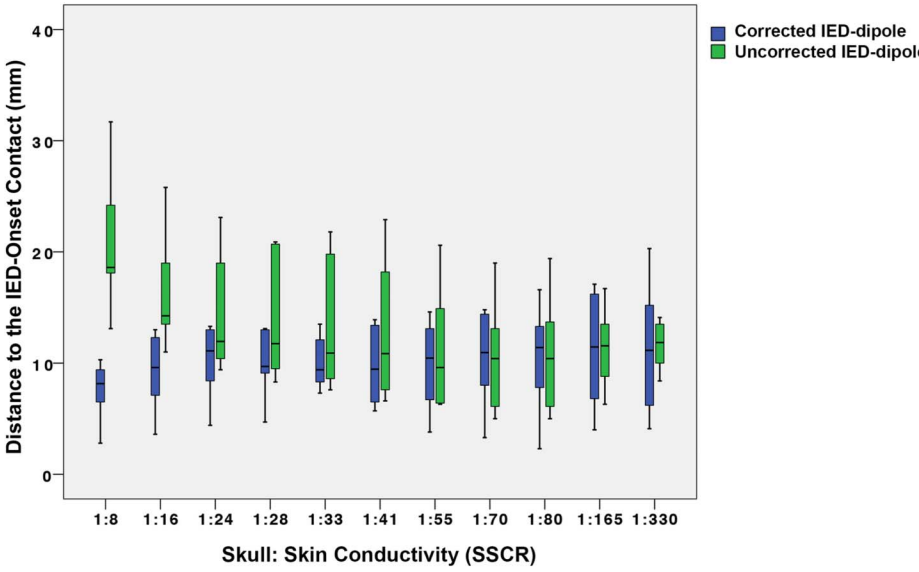

FIG. 6. Boxplots showing distances from corrected IED-dipoles (*blue/dark*) versus uncorrected IED-dipoles (*green/light*) to the IED-onset contacts. Using various SSCR from 1:8 to 1:330, the distance from corrected IED-dipoles to the IED-onset contacts were insignificantly different ($P = 0.1$). However, using SSCR 1:8 to 1:28, distances from uncorrected IED-dipoles to the IED-onset contacts increased significantly ($P < 0.001$–0.02). Using SSCR of 1:8 and 1:16, distances from corrected IED-dipoles were significantly smaller compared with distances from uncorrected IED-dipoles to the IED-onset contacts ($P = 0.03$ for both SSCR).

The difference between our ESI results of temporal IED and the study by Wennberg and Cheyne[15] may derive from several technical reasons. They found the presumed sources of anterior temporal spikes using equivalent current dipole as a source model localized within 14–76 mm of the spike generator, defined by intracerebral EEG. Our results show a considerably smaller localization error even before applying the individual iEV. This smaller localization error can be explained by (1) the higher number of scalp electrodes applied in our study, (2) our use of different skull conductivities, and (3) application of a four-compartment finite element head model that also included modeling the high conductivity of the cerebrospinal fluid.[16,17] Moreover, we estimated the cortical extents of IED generators in the subgroup of anterior temporal IED by observing the amplitude fall-off of IEDs. The maximal distance from the stereo-EEG contact recording an amplitude of approximately 70 μV to the corrected IED-dipoles was calculated as the radius for cortex involvement. Based on this calculation, our median cortical extent of generators (16.5 cm^2) fell in the range of 10 to 20 cm^2 of synchronous or temporally overlapping cortex activation, required for 90% of temporal IED to be present on scalp EEG reported by a previous study using simultaneous subdural and scalp EEG.[14]

We further investigated the correlation between distances to stereo-EEG IED-onset contacts from corrected IED-dipoles and IED amplitudes. To the best of our knowledge, this correlation in humans is not available in the current literature. Previously, various methods have been applied to evaluate intracerebral electrode sensitivity and determine distance to neuronal source. Zaveri et al.[18] found that the magnitude of the electrical field intensity of a static point charge decreases with increasing distance from its position. Likewise, numerical simulations have shown that the magnitude of electrical field intensity or the amplitude (a) of generator signals dropped dramatically within the first few millimeters of increasing recording distance (d) ($a(d) \propto 1/d^{1\text{-}2}$).[19] With larger distances, further amplitude decreases were seemingly less pronounced. We observed similar correlations ($a(d) \propto 1/d^b$) with b values between 0.8 and 2.3 in our patients, using the location of corrected IED-dipoles as sources, which is concordant with the results from simulations. In addition, von Ellenrieder et al.[19] found that the larger amplitude of synchronized generators ($a(d) \propto 1/d$) decline slower compared with unsynchronized generators ($a(d) \propto 1/d^2$). This corresponds to the correlations we observed in the anterior temporal IED cluster ($a(d) \propto 1/d^{1.5}$) and the prefrontal IED cluster ($a(d) \propto 1/d^{2.2}$). The variation of the power (variable b) is possibly related to the degree of synchronization, extent of IED generators, or histological characteristics of epileptogenic tissue.

Surprisingly, the effect of different skull conductivities (SSCR from 1:8–1:330) was clearly seen on the distances from uncorrected IED-dipole but not from corrected IED-dipoles to the IED-onset contact. We expected that using low skull conductivities (SSCR higher than 1:80) would result in significantly larger localization error for the corrected IED-dipoles. A possible explanation is that the effect of varying skull conductivities on ESI localization error of ESP and IED was cancelled out after applying individual iEV. SSCR 1:8 to 1:80 are standard adult skull:skin conductivity ratios in three-compartment head models.[20] However, lower skull conductivity were also found in recent six-compartment calibration studies, and even much higher e.g., 1:180 have also been reported.[21–25] In summary, tissue conductivities remain a source of uncertainty and will need to be further taken into account in our individual iEV methodology and, more generally, in ESI.[9]

Dipole modeling is a relatively simple way to model the source of human brain activity.[26] Like other inverse methods, dipole modeling suffers from the fact that possible solutions outnumber the measured values, given that the different cortical sources could produce the same electrical field. The focal dipole is fitted to active cortical sources with spatial extent and complex configuration; the dipole therefore is placed deeper to represent the scalp voltage field produced by extended cortical sources.[27,28] The resulting localization of dipole modeling should be interpreted as centers of gravity [of current sources (+) and sinks

(−)], summarizing the surrounding activity. The dipole locates at an equivalent center below the cortical generator, whereas its orientation points to the active cortical patch. There are two reasons for applying dipole modeling in our analysis: (i) ESP potentials, as substrates for calculation of the error vector, are focal (point like) sources, dipole modeling was used, as this has been shown to provide higher localization accuracy than distributed methods.[29] For the IED, which subsequently was subtracted by the error vector, we applied the same inverse method as, in our opinion, the resulting localization errors of both activities would be comparable i.e., no additive error, resulting from using different inverse solutions. (ii) Despite the above-mentioned limitation, the clinical value of ESI of epileptic discharges using dipole modeling in the presurgical evaluation has been demonstrated to outperform distributed methods at the sublobar level when epileptogenic zones defined by stereo-EEG were used as a gold standard.[4,5,30–33]

In this study, we determined the systematic error vector map of ESI based on a state-of-the-art four-compartment (skin, skull, CSF, brain) realistic head model, using stimulation potentials (ESP) of known sources in a group of epilepsy patients. We then applied the determined map in a postprocessing step to correct the overall results of source localization of IED using the same head modeling approach. We acknowledge the following limitations:

1. The iEV was specific to the individual, area of the brain, source depth, four-compartment volume conduction and source modeling method (dipole fitting), tissue conductivities/anisotropies, and the like.[9,10,34] Nevertheless, in patient no. 2, we successfully applied the iEV obtained from the right anterior temporal area to uncorrected IED-dipole originated in the left anterior temporal area. Our future plan is to develop regional specific (sublobar region-matched and depth-matched) iEV and area-specific (area-matched, age-matched and gender-matched) iEV that can be applied in respective patients in whom the source of IED are not known. In principle, other source modeling methods consisting of dipole source model, e.g., CLARA, could potentially benefit from an iEV strategy. However, this would have to be tested.
2. We used high number of monomorphic IEDs with high signal-to-noise ratio to achieve a good model fit in ESI. Future work also needs to include ictal patterns, which often have a small number of less monomorphic discernible potentials with a lower signal-to-noise ratio.
3. We have to expect that source localization errors of IED before application of iEV might partly be due to fitting a focal dipole source to a more extended IED source patch, which will result in a depth localization error.[35] Our iEV cannot compensate for such mismodeling of source extent.

Outcome and prognosis after surgical resection clearly depend on the extent of resection guided by intracerebral EEG.[36] Here, we describe an empirical method to better estimate the location of neuronal sources of IED that would help to outline surgical resections, especially in nonlesional cases, or to plan further intracerebral electrode placement. In both the explorative and the confirmative scenario, precision of ESI is a prerequisite for successful intracerebral workup and all resulting decision making. Therefore, we should aim at ESI precision in the range of <10 mm from the epileptic discharge generator. The presented method to correct EEG source localization of IED by applying individual iEV, derived from electrical stimulation at the contact closest to the invasively generated focus hypothesis may contribute to achieve this precision.

CONCLUSIONS

Application of individual inverted error vector improves current standard EEG source localization results of interictal epileptic discharges. This may optimize planning of presurgical intracerebral EEG evaluation and surgical treatment in pharmacoresistant epilepsy, in particular in nonlesional cases.

ACKNOWLEDGMENTS

The authors thank Nina Spedt, Cindy Gebhardt and Michael Schlüter for expert technical assistance.

REFERENCES

1. Isnard J, Taussig D, Bartolomei F, et al. French guidelines on stereo-electroencephalography (SEEG). Neurophysiol Clin 2018;48:5–13.
2. Wehner T, Unnwongse K, Wellmer J. How are patients selected for intracranial EEG recordings? In: Axmacher N, Intracranial EEG, eds. Studies in Neuroscience, Psychology and Behavioral Economics. Cham: Springer, 2023; 3–18.
3. Foged MT, Martens T, Pinborg LH, et al. Diagnostic added value of electrical source imaging in presurgical evaluation of patients with epilepsy: a prospective study. Clin Neurophysiol 2020;131:324–329.
4. Barborica A, Mindruta I, Sheybani L, et al. Extracting seizure onset from surface EEG with independent component analysis: insights from simultaneous scalp and intracerebral EEG. Neuroimage Clin 2021;32:102838.
5. Cox BC, Danoun OA, Lundstrom BN, Lagerlund TD, Wong-Kisiel LC, Brinkmann BH. EEG source imaging concordance with intracranial EEG and epileptologist review in focal epilepsy. Brain Commun 2021;3:fcab278.
6. Beniczky S, Rosenzweig I, Scherg M, et al. Ictal EEG source imaging in presurgical evaluation: high agreement between analysis methods. Seizure 2016;43:1–5.
7. Mălîia MD, Meritam P, Scherg M, et al. Epileptiform discharge propagation: analyzing spikes from the onset to the peak. Clin Neurophysiol 2016;127:2127–2133.
8. Song J, Davey C, Poulsen C, et al. EEG source localization: sensor density and head surface coverage. J Neurosci Methods 2015;256:9–21.
9. Vorwerk J, Wolters CH, Baumgarten D. Global sensitivity of EEG source analysis to tissue conductivity uncertainties. Front Hum Neurosci 2024;18:1335212.
10. Unnwongse K, Rampp S, Wehner T, et al. Validating EEG source imaging using intracranial electrical stimulation. Brain Commun 2023;5:fcad023.
11. Huppertz HJ, Grimm C, Fauser S, et al. Enhanced visualization of blurred gray-white matter junctions in focal cortical dysplasia by voxel-based 3D MRI analysis. Epilepsy Res 2005;67:35–50.
12. Gloor P. Neuronal generators and the problem of localization in electroencephalography: application of volume conductor theory to electroencephalography. J Clin Neurophysiol 1985;2:327–354.
13. Wennberg RA, Lozano AM. Intracranial volume conduction of cortical spikes and sleep potentials recorded with deep brain stimulating electrodes. Clin Neurophysiol 2003;114:1403–1418.

14. Tao JX, Ray A, Hawes-Ebersole S, Ebersole JS. Intracranial EEG substrates of scalp EEG interictal spikes. Epilepsia 2005;46:669–676.
15. Wennberg R, Cheyne D. EEG source imaging of anterior temporal lobe spikes: validity and reliability. Clin Neurophysiol 2014;125:886–902.
16. Rice JK, Rorden C, Little JS, Parra LC. Subject position affects EEG magnitudes. Neuroimage 2013;64:476–484.
17. Piastra MC, Nüßing A, Vorwerk J, Clerc M, Engwer C, Wolters CH. A comprehensive study on electroencephalography and magnetoencephalography sensitivity to cortical and subcortical sources. Hum Brain Mapp 2021;42:978–992.
18. Zaveri HP, Duckrow RB, Spencer SS. Concerning the observation of an electrical potential at a distance from an intracranial electrode contact. Clin Neurophysiol 2009;120:1873–1875.
19. von Ellenrieder N, Khoo HM, Dubeau F, Gotman J. What do intracerebral electrodes measure? Clin Neurophysiol 2021;132:1105–1115.
20. McCann H, Pisano G, Beltrachini L. Variation in reported human head tissue electrical conductivity values. Brain Topogr 2019;32:825–858. [published correction appears in Brain Topogr. 2021 Jan;34(1):110-115].
21. Antonakakis M, Schrader S, Aydin Ü, et al. Inter-subject variability of skull conductivity and thickness in calibrated realistic head models. Neuroimage 2020;223:117353.
22. Neugebauer F, Antonakakis M, Unnwongse K, et al. Validating EEG, MEG and combined MEG and EEG beamforming for an estimation of the epileptogenic zone in focal cortical dysplasia. Brain Sci 2022;12:114.
23. Aydin Ü, Vorwerk J, Dümpelmann M, et al. Combined EEG/MEG can outperform single modality EEG or MEG source reconstruction in presurgical epilepsy diagnosis. PLoS One 2015;10:e0118753.
24. Aydin Ü, Rampp S, Wollbrink A, et al. Zoomed MRI guided by combined EEG/MEG source analysis: a multimodal approach for optimizing presurgical epilepsy work-up and its application in a multifocal epilepsy patient case study. Brain Topogr 2017;30:417–433.
25. Antonakakis M, Kaiser F, Rampp S, et al. Targeted and optimized multichannel transcranial direct current stimulation for focal epilepsy: an N-of-1 trial. Brain Stimul 2024;17:221–223.
26. de Munck JC, van Dijk BW, Spekreijse H. Mathematical dipoles are adequate to describe realistic generators of human brain activity. IEEE Trans Biomed Eng 1988;35:960–966.
27. Kobayashi K, Yoshinaga H, Ohtsuka Y, Gotman J. Dipole modeling of epileptic spikes can be accurate or misleading. Epilepsia 2005;46:397–408.
28. Singh J, Ebersole JS, Brinkmann BH. From theory to practical fundamentals of electroencephalographic source imaging in localizing the epileptogenic zone. Epilepsia 2022;63:2476–2490.
29. Pascarella A, Mikulan E, Sciacchitano F, et al. An in-vivo validation of ESI methods with focal sources. Neuroimage 2023;277:120219.
30. Koessler L, Benar C, Maillard L, et al. Source localization of ictal epileptic activity investigated by high resolution EEG and validated by SEEG. Neuroimage 2010;51:642–653.
31. Rikir E, Koessler L, Gavaret M, et al. Electrical source imaging in cortical malformation-related epilepsy: a prospective EEG-SEEG concordance study. Epilepsia 2014;55:918–932.
32. Sharma P, Scherg M, Pinborg LH, et al. Ictal and interictal electric source imaging in pre-surgical evaluation: a prospective study. Eur J Neurol 2018;25:1154–1160.
33. Abdallah C, Maillard LG, Rikir E, et al. Localizing value of electrical source imaging: frontal lobe, malformations of cortical development and negative MRI related epilepsies are the best candidates. Neuroimage Clin 2017;16:319–329. Published 2017 Aug 8.
34. Wolters CH, Anwander A, Tricoche X, Weinstein D, Koch MA, MacLeod RS. Influence of tissue conductivity anisotropy on EEG/MEG field and return current computation in a realistic head model: a simulation and visualization study using high-resolution finite element modeling. Neuroimage 2006;30:813–826.
35. Lucka F, Pursiainen S, Burger M, Wolters CH. Hierarchical Bayesian inference for the EEG inverse problem using realistic FE head models: depth localization and source separation for focal primary currents. Neuroimage 2012;61:1364–1382.
36. Kim DW, Kim HK, Lee SK, Chu K, Chung CK. Extent of neocortical resection and surgical outcome of epilepsy: intracranial EEG analysis. Epilepsia 2010;51:1010–1017.